17th International Conference on Microwave and High Frequency Heating
Valencia, Spain, September 9-12, 2019
AMPERE 2019
ISBN: 978-84-9048-719-8
DOI: http://dx.doi.org/10.4995/Ampere2019.2019.9782

AUTOMATIC MEASUREMENT OF MAGNETRON RIEKE DIAGRAMS

V. Bilik[1]

[1]*Faculty of Electrical Engineering and Information Technology, Slovak University of Technology, Ilkovicova 3, 81219 Bratislava, Slovak Republic*
vladimir.bilik@s-team.sk

Keywords: Rieke diagram, magnetron, high-power vector reflectometer

Introduction

One of the most important characteristics of a magnetron is its *Rieke diagram* [1], [2]. The diagram visualizes the dependence of the generated frequency f_g and the net power P_L delivered to load on a specifically defined magnetron load reflection coefficient Γ_R. The diagram is a (rotated) polar chart in the complex plane of Γ_R, plotted as a family of isolines of constant f_g and of constant P_L (Fig. 1). Rieke diagrams are essential in the design of magnetrons and in magnetron applications without isolators, such as domestic or professional microwave ovens.

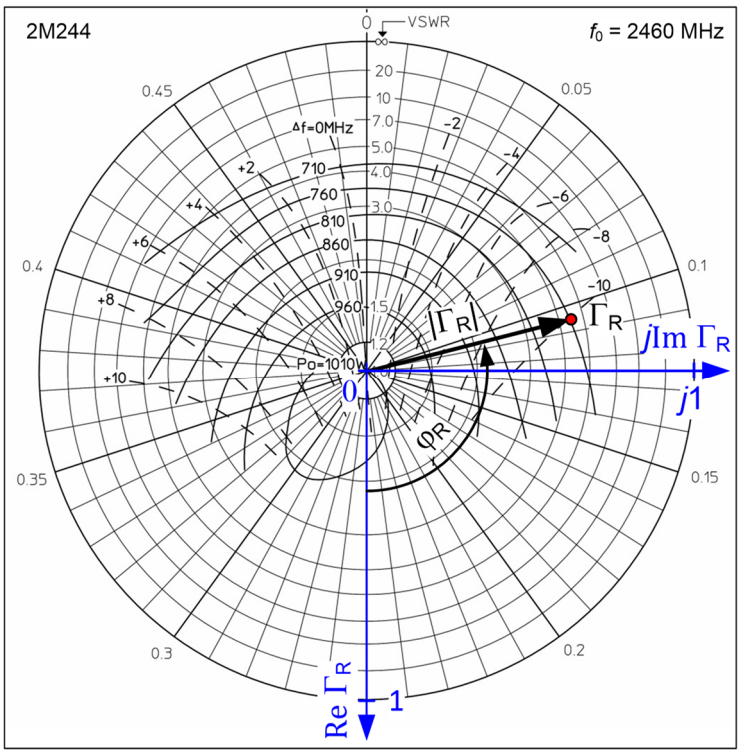

Fig. 1. Example Rieke diagram.

Traditionally, the construction of Rieke diagrams (see e.g. [1], [3], [4]) has been a tedious and time-consuming task that requires highly specialized equipment. This has prevented

systematic studies of the dependence of Rieke diagrams on operating conditions, such as, for example, anode current and its ripple, filament current, and mounting repeatability.

We have devised a procedure centered around a standard, commercially available, high-power automatic impedance matching device (autotuner). This procedure enables fully automatic measurement and plotting of the isolines of choice. The measurement process consists of stepping through a grid of n suitably predetermined reflection coefficients Γ_R, covering a desired area of the polar chart. Each Γ_R is measured accurately by the autotuner, along with the corresponding f_g and P_L. A dedicated MATLAB routine then reads this raw data, approximates them by 2-dimensional splines, and uses the splines to plot smoothed isocontours for chosen constant values of f_g and P_L, thus completing the Rieke diagram construction. In what follows, we present the details of this procedure as well as a real-life example.

Reference Launcher

A magnetron's Rieke diagram-related load reflection coefficient, conveniently named the *Rieke reflection coefficient* [3]

$$\Gamma_R = x_R + jy_R = |\Gamma_R| \exp(j\varphi_R)$$

is defined as the reflection coefficient observed looking toward the load in an agreed magnetron-to-rectangular-waveguide coupling structure called the *reference launcher* (Fig. 2). The launcher is characterized by three main parameters: the waveguide inner dimensions a_r (not shown in Fig. 2) and b_r, and the distance d_s of the magnetron antenna axis from the short-circuited waveguide end. The distance d_R between the antenna axis and the waveguide output is not critical; it should only be long enough to sufficiently attenuate higher-order modes potentially excited by the antenna. Conceptually, the reference launcher can serve to directly measure Γ_R, as shown in Fig. 2b.

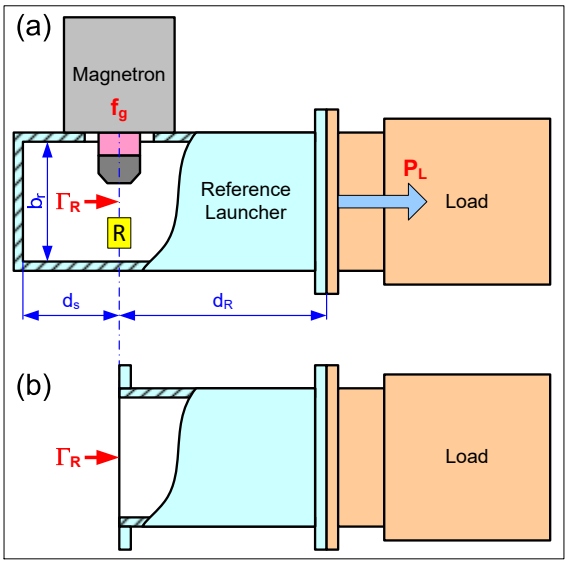

Fig. 2. a) Magnetron in reference launcher. b) Definition of Rieke reflection coefficient Γ_R.

Basic reference launcher dimensions for 2.45-GHz magnetrons with powers up to about 2 kW have been standardized by the Electronic Industries Association of Japan (EIAJ). The launcher uses a waveguide with the inner dimensions a_r = 95.3 mm and b_r = 54.6 mm. We will refer to it as the *launcher waveguide* (LWG). The antenna-short distance is d_s = 18.6 mm. The antenna-flange distance $d_R \geq 150$ mm ensures that the attenuation of the lowest higher-order mode (TE01) exceeds 33 dB.

Experimental Setup

A block diagram of the experimental setup is shown in Fig. 3a. The magnetron under test is coupled to a reference launcher and fed from a high-voltage DC power supply. A low-reflection transition (taper) connects the launcher with the standard WR340 waveguide autotuner. The autotuner is terminated in a high-power matched load, such as a waterload. In this configuration, the autotuner can accomplish a task inverse to impedance matching: realizing any desired Rieke reflection coefficient Γ_R. During the measurement process, the autotuner accurately measures each Γ_R it produces, along with the corresponding generated frequency f_g and net delivered power P_L. These are the three data a collection of which is necessary for creating a Rieke diagram. The whole process is controlled from an external computer (PC).

The setup is fairly simple: the only specialized components required are the reference launcher and the tapered LWG-to-WR340 transition[1].

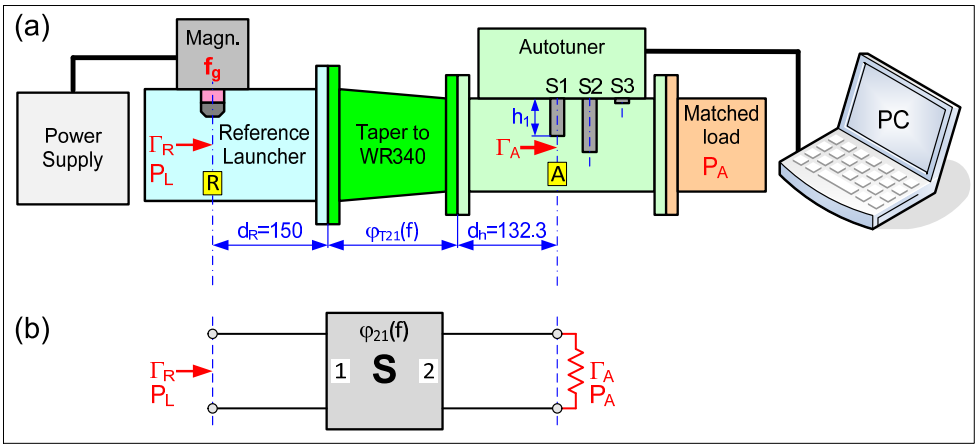

Fig. 3. Rieke diagram measurement setup.

Reflection Coefficient and Delivered Power Transformation

The high-power vector reflectometer incorporated in the autotuner inherently measures the reflection coefficient Γ_A at a reference plane A as well as the net power P_A absorbed in the load. In order to compute Γ_R and P_L, we need to know the scattering matrix $\boldsymbol{S}$ of the circuit between planes R and A (Fig. 3b). The transform is accomplished by the formulas [7]

[1] For measurements with magnetron antenna probes, an LWG-based calibration kit is also required [5], [6].

$$\Gamma_R = S_{11} + \frac{S_{12}S_{21}\Gamma_A}{1 - S_{22}\Gamma_A} = \frac{S_{11} - D\Gamma_A}{1 - S_{22}\Gamma_A} \tag{1}$$

$$P_L = P_A \frac{\left|1 - S_{22}\Gamma_A\right|^2 - \left|S_{11} - D\Gamma_A\right|^2}{\left|S_{21}\right|^2 \left(1 - \left|\Gamma_A\right|^2\right)} \tag{2}$$

where $D = S_{11}S_{22} - S_{12}S_{21}$ is the determinant of the ***S***-matrix. The inverse transform to (1) is

$$\Gamma_A = \frac{\Gamma_R - S_{11}}{S_{22}\Gamma_R - D} \tag{3}$$

In our case (a typical situation), the circuit between planes R and A is a cascade of a launcher waveguide section with length d_R, a well-matched LWG-to-WR340 transition, and a section of WR340 waveguide with length d_h. Neglecting the circuit losses and mismatches (justified for a properly designed transition) the S-parameters are

$$S_{11} = 0; \qquad S_{22} = 0; \qquad S_{12} = S_{21} = \exp\left(j\varphi_{21}\right) \tag{4}$$

which results in

$$\Gamma_R = \Gamma_A \exp\left(j2\varphi_{21}\right); \qquad P_L = P_A \tag{5}$$

reducing the transform to merely a phase-shifting (rotation) of Γ_A. The S_{21} phase angle is

$$\varphi_{21}(f) = -\frac{2\pi d_R}{\lambda_{gr}} + \varphi_{T21} - \frac{2\pi d_h}{\lambda_g} \tag{6}$$

where λ_{gr} is the launcher guide wavelength, λ_g is the WR340 guide wavelength, and φ_{T21} is the taper transmission coefficient phase. All three quantities are frequency-dependent.

The usefulness of expressing the conversion in terms of *S*-parameters lies in the fact that the PC program controlling the measurement process is capable of loading a text file with tabulated frequency dependence of S_{ij}, performing the mappings (1) and (2) internally, and then immediately outputting the Rieke reflection coefficient Γ_R and the delivered power P_L.

Realizing Reflection Coefficients

The procedure of obtaining a Rieke diagram calls for realizing a sufficiently dense set of predetermined Rieke reflection coefficients Γ_R, and consequently, autotuner input reflection coefficients Γ_A. Any Γ_A within the tuner's capability can be realized by proper tuning stub insertions h_1, h_2, h_3 of a match-terminated autotuner. The method of determining the insertions is intimately linked with the autotuning algorithm. An equivalent circuit for an impedance matching arrangement with a matched generator ($\Gamma_G = 0$) is shown in Fig. 4. The tuner is a loss-free adjustable circuit characterized by its S-matrix $\boldsymbol{S_A}$ defined for reference planes 1 and 2. A load with reflection coefficient Γ_3 is connected at plane 3, that is usually separated from plane 2 by a transmission line with electric length θ. To achieve a matching of load Γ_3, the tuner must be adjusted so that its input reflection coefficient is $\Gamma_1 = 0$. The theory [8] proves that in this case, the condition $\Gamma_2 = (\Gamma_x)^*$ is satisfied at plane 2, where Γ_2 is seen looking into port 2 of the tuner and $\Gamma_x = \Gamma_3 \exp(-j2\theta)$ is seen looking toward the load. The asterisk indicates the complex conjugation. In fact, Γ_2 is the reflection coefficient "realized" by the reversed tuner. The matched termination at the other port (port 1) is

provided by the generator. Based on these facts, the following algorithm can be formulated for realizing any input reflection coefficient Γ_A:

- Choose a desired input reflection coefficient Γ_A and frequency f.
- Run the autotuning algorithm, using as input values the conjugated and rotated reflection coefficient

$$\Gamma_3 = \Gamma_A^* \exp(j2\theta) \tag{7}$$

  and frequency f. The algorithm will output the tuning stub insertions h_{1m}, h_{2m}, h_{3m}.
- "Reverse" the tuner, i.e. set the tuning stubs to insertions $h_1 = h_{3m}$, $h_2 = h_{2m}$, $h_3 = h_{1m}$. Then the tuner input reflection coefficient at frequency f will be $\Gamma_1 = \Gamma_A$.

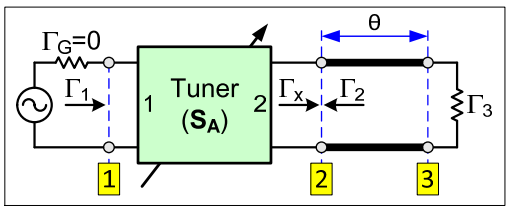

Fig. 4. Equivalent circuit for an impedance matching arrangement.

Rieke Diagram Measurement Procedure

The procedure for obtaining a Rieke diagram consists of the following basic steps:

1. Define a grid of Rieke reflection coefficients Γ_{Ri}, $i = 1\ldots n$, that cover with a sufficient density the desired area of the polar chart. The grid need not be regular; it can be, for instance, finer wherever we need a greater detail.
2. Using (3), create from Γ_{Ri} a set of corresponding tuner input reflection coefficients Γ_{Ai}, $i = 1\ldots n$, to be realized by the autotuner.
3. Create the *stubs motion scenario*: a sequence $\{\boldsymbol{h}\}_i \equiv \{h_1, h_2, h_3\}_i$, $i = 1\ldots n$, of autotuner stub insertions realizing the set Γ_{Ai}.
4. Run the scenario, i.e. step through the sequence $\{\boldsymbol{h}\}_i$, $i = 1\ldots n$, and, for each setting:
   a) Move the tuning stubs to the corresponding insertions.
   b) Use the autotuner to measure the reflection coefficient Γ_A, the generated frequency f_g, and the power P_A absorbed in the load (note that the measured Γ_A will generally differ from the scenario value).
   c) Transform Γ_A to the Rieke reflection coefficient Γ_R, and transform P_A to the net power P_L delivered by the magnetron. For all practical purposes, the simplified equations (4) – (6) are appropriate for this purpose.

   In this way, raw data for constructing a Rieke diagram are obtained. The data is a collection of n triplets $\{\Gamma_R, f_g, P_L\}_i$, $i = 1\ldots n$, with $\Gamma_R = x_R + jy_R$ being, in general, scattered irregularly and arbitrarily in the complex plane.
5. Choose a range of constant values of f_g and of P_L for which the Rieke diagram isolines should be drawn.
6. Apply a mathematical routine that
   a) uses the acquired data to create tabulated functions $f_g = f(x_R, y_R)$, $P_L = f(x_R, y_R)$; and

b) approximates the two obtained functions by a 2D smoothing spline surface each.

7. Using the approximations, make plots of smoothed isocontours for the chosen values of f_g and P_L, thus completing the desired Rieke diagram construction.

We have developed a dedicated MATLAB routine that implements steps 6 and 7.

Experiments

To illustrate the developed procedure, we performed experiments using a Panasonic 2M244 magnetron (nominal frequency f_0 = 2460 MHz, nominal power into a match P_0 = 1010 W). The datasheet Rieke diagram (Fig. 1) was reportedly obtained using a single-phase full-wave rectifier without filter, with peak anode voltage 4.35kV. However, in our experiments, we used an available single-phase half-wave rectifier that was only able to reach 900 W rather than the rated magnetron power P_0. The time dependence $P_L(t)$ of power delivered to a matched load is shown in Fig. 5.

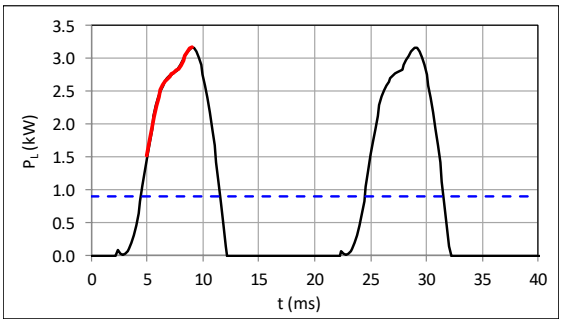

Fig. 5. Time dependence of power P_L delivered to a matched load. Dashed line – mean power (900 W). Red portion – frequency counting interval.

A photograph of the experimental setup is shown in Fig. 6; it corresponds to the block diagram of Fig. 3. The setup employs an S-TEAM WR340 autotuner STHT 1.6. Results of each individual measurement were obtained by processing 201 samples taken over 40 ms, i.e. two periods of the power waveform shown in Fig. 5. Frequency was averaged over the red-highlighted 4-ms interval. To improve the terminating match, we preceded the waterload by an auxiliary tuner with fixed stub insertions.

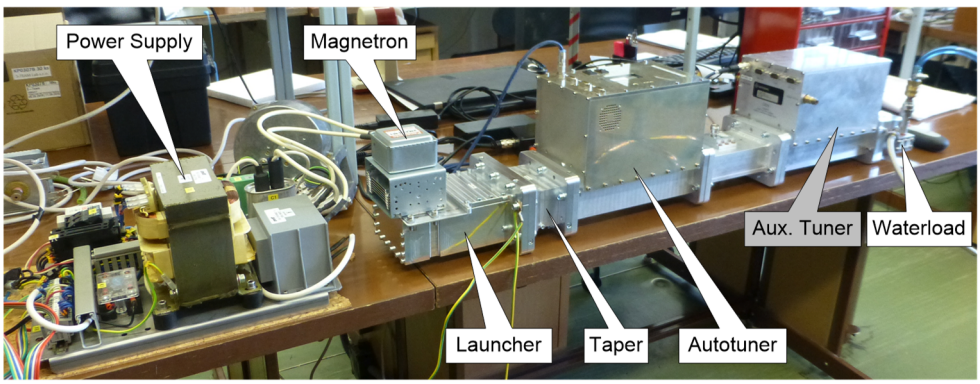

Fig. 6. Experimental setup.

We used a linear taper with optimized length 82.5 mm. We determined its scattering parameters S_{Tij} in the 2400 – 2500 MHz range by both electromagnetic simulation and measurement. The difference of the transmission phase φ_{T21} was below 1.4°. The measured magnitude $|S_{T21}|$ deviates from theoretical unity by less than 0.005; the input mismatches $|S_{T11}|$ and $|S_{T22}|$ are below 0.01. Therefore, the assumptions $|S_{T21}| = 1$ and $|S_{T11}| = |S_{T22}| = 0$ were justified.

We implemented the transformation matrix $\boldsymbol{S}$ (Fig. 3) by applying (4) and (6) for frequencies in the range 2400 – 2500 MHz in 1-MHz increments, and storing the results in a text file that was then read in by the PC controller SW.

To ready the system for repeated Rieke diagram measurements, we prepared a rectangular grid of tuner input reflection coefficients Γ_A with maximal magnitude 0.7 and step 0.05 in both dimensions (Fig. 7a). We used the resulting $n = 614$ values in the control SW to generate the corresponding stubs motion scenario for an assumed frequency of 2460 MHz.

During the measurement process, the control SW steps through the scenario. For each step, the stubs are moved to the prescribed insertions, and then a wait period (in our case 300 ms) is introduced to allow the magnetron to settle. Then, a "burst" of measurements (in our case 10 of them) is made and recorded. This cycle is repeated for the whole scenario. For our settings, the complete process took about 24 minutes. All individual results are stored in a text file (in our case 10 × 614 data lines) for detailed process analysis. In addition, a separate ".rkd" text file was created with only $n = 614$ data lines, each containing the burst averages and standard deviations for the quantities of interest (Γ_R, f_g, and P_L). These averages are the actual input data to be used for creating the Rieke diagram; the deviations are useful for detecting possible magnetron instabilities (e.g. jumps in frequency and power).

An example of a measured collection of the Rieke reflection coefficients, as stored in an rkd file, is shown in Fig. 7b. Evidently, the data tend to be "expelled" from the magnetron sink area, where the generated frequency is very sensitive to load variations.

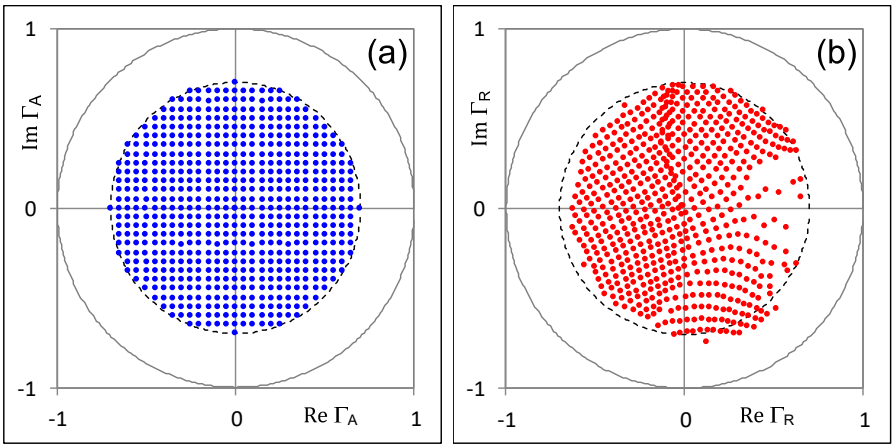

Fig. 7. a) – A grid of desired tuner input reflection coefficients Γ_A; b) – A corresponding set of measured Rieke reflection coefficients Γ_R.

We used the generated rkd file as an input to a MATLAB program implementing steps 6 and 7 of the procedure outlined above. Fig. 8 shows examples of the input data and their approximation by 2D smoothing spline surfaces, as obtained by the MATLAB function

tpaps. Using the approximations, smoothed isocontours (horizontal cuts of the surfaces in Fig. 8) can be plotted (e.g. via the MATLAB function contour) for any desired constant value of P_L and Γ_R (solid curves in Fig. 9).

In a similar way, we processed a digitized datasheet Rieke diagram (dashed lines in Fig. 9). The measured and datasheet patterns manifest general similarity but also significant discrepancies. The most likely reason may be the insufficient DC power supply that we used. For explanation of the differences, a systematic study is required but is beyond the scope of this paper. Nevertheless, we have provided an efficient tool that enables, among others, studies of this kind.

Conclusions

We have developed an experimental setup, a measurement procedure, and a MATLAB data processing program that enable fully automatic measurement and plotting of magnetron Rieke diagrams. The fundamental component of the workplace is a standard, commercially available, high-power autotuner. After a one-time processing for preparation of the necessary text files (transformation ***S***-matrix and stubs motion scenario), the measurement is a matter of practically a single button click. Depending on the length of the scenario, the data acquisition process takes typically several tens of minutes, with no involvement required from the operator. Given the data, smoothed Rieke diagram contours can be generated practically immediately.

The proposed system and methodology have the potential to enable systematic statistical studies of the dependence of Rieke diagrams on magnetron operating conditions, for which mass data collection and rapid evaluation are essential.

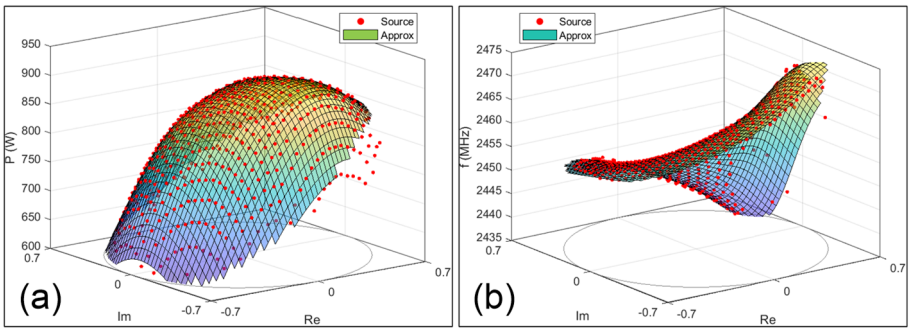

Fig. 8. Input data (red dots) and their spline approximation for (a) delivered power P_L and (b) generated frequency f_g. The bottom surface is Γ_R-plane.

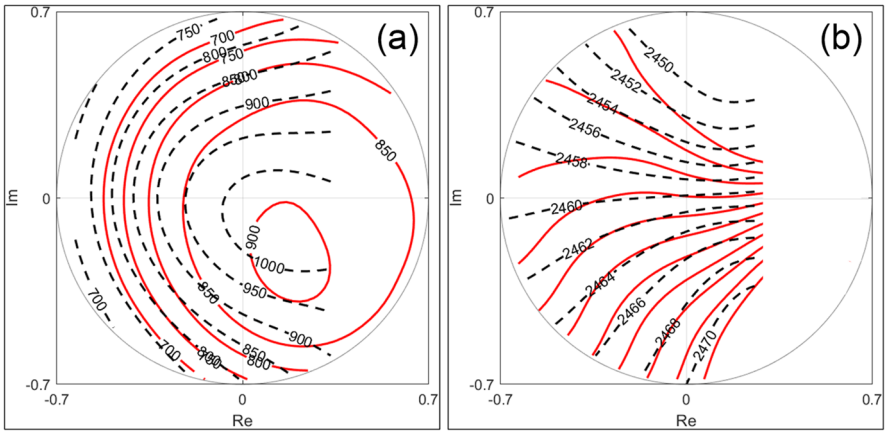

Fig. 9. Rieke diagram contours for (a) delivered power P_L and (b) generated frequency f_g. The dashed lines correspond to the 2M244 magnetron datasheet.

References

1. Smith, G., *Microwave Magnetrons*, MIT RadLab Series, Vol. 6, New York: McGraw-Hill, 1948, Sec. 7-5, 18-9.
2. Meredith, R. J., *Engineers' Handbook of Industrial Microwave Heating*, London: The IEE, 1998, Sec. 9.3.
3. Takahashi, H., I. Namba, K. Akiyama, *J. Microwave Power*, 1979, **14**, 261–267.
4. Yixue, W., Z. Zhaotang, *Proc. ICMMT'98*, 1998, 795–798.
5. Bilik, V, *Proc. 3rd Global Congress on Microwave Energy Applications 3GCMEA*, 2016.
6. Bilik, V, *Proc. 16th Int. Conf. on Microwave and High Frequency Heating AMPERE,* 2017.
7. Engen, G., *Microwave Circuit Theory and Foundations of Microwave Metrology*, London: P. Peregrinus, 1992, 15–39.
8. Bilik, V, *Proc. 48th Annual Microwave Power Symposium IMPI 48*, 2014, 6-9.